Chinese Chemical Letters 36 (2025) 109712

Contents lists available at ScienceDirect

Chinese Chemical Letters

journal homepage: www.elsevier.com/locate/cclet

# Rational design of highly conductive and stable 3D flexible composite current collector for high performance lithium-ion battery electrodes

Huanyan Liu[a], Jiajun Long[a,b], Hua Yu[b], Shichao Zhang[c], Wenbo Liu[a,*]

[a] School of Mechanical Engineering, Sichuan University, Chengdu 610065, China
[b] School of New Energy and Materials, Southwest Petroleum University, Chengdu 610500, China
[c] School of Materials Science and Engineering, Beihang University, Beijing 100191, China

ARTICLE INFO

*Article history:*
Received 15 December 2023
Revised 8 January 2024
Accepted 1 March 2024
Available online 7 March 2024

*Keywords:*
Lithium-ion battery
Composite current collector
Highly conductive electrode
High performance
Metal sulfide

ABSTRACT

Anode active materials involving transition metal oxides and sulfides are of great significance for high energy density lithium-ion batteries (LIBs), but the huge volume expansion and inferior electronic conductivity upon cycling critically constrain their further application. Herein, from a new perspective, a highly conductive and stable 3D flexible composite current collector is rationally designed by facilely electrodepositing metallic Ni thin layer onto the carbon cloth (CC/Ni), which endows the supported active materials with exceptional electronic conductivity and structural stability. In addition, the homogeneously distributed metallic Ni protrusions external CC can strongly bond with the active components, ensuring the structural integrity of electrodes upon cycling. More importantly, the 3D network structure with large specific surface area provides abundant space to alleviate the volume expansion and more active sites for electrochemical reactions. Therefore, taking $Ni_3S_2$ nanosheet ($Ni_3S_2$ NS) anode as an example, the prepared $Ni_3S_2$ NS@CC/Ni electrode shows a high specific capacity of 2.32 mAh/cm$^2$ at 1 mA/cm$^2$ and high capacity retention of 1.68 mAh/cm$^2$ at a high rate of 8 mA/cm$^2$. This study provides a universal approach to obtain highly conductive and stable 3D flexible current collectors towards high performance metal-ion batteries beyond LIBs.



With the rising demand for various industrial products including electronic devices and electric vehicles, lithium-ion batteries (LIBs) have received unprecedented attention as the leading energy storage system in current commercial application scenarios [1–3]. However, the specific capacity of the commercial graphite anode is only 372 mAh/g, which calls for other alternative anode materials [4,5]. As a result, transition metal oxides (*e.g.*, $SnO_x$, $CuO_x$, $FeO_x$, $CoO_x$, $NiO_x$) and sulfides (*e.g.*, $CuS_x$, $FeS_x$, $CoS_x$, $NiS_x$, $SnS_x$) with rich redox chemistry have been exploited as potential anodes for next-generation high-performance LIBs due to their high theoretical specific capacity and appropriate Li-insertion voltage [6–17]. Nevertheless, their further practical application and commercial evolution was crucially constrained by the huge volume expansion and inferior electronic conductivity upon repeated cycling, which leads to poor cycling and rate performance [18,19]. Lots of attentions have been focused on the design of anode materials, such as fabricating nano-structured materials, manufacturing hollow or porous structures, and composite with conductive substances [20–25]. It should be noted that all materials need to be attached to current collectors before being assembled into batteries. Current collectors with rich conducting networks can bridge the inner battery and external circuit, leading to reduced battery internal resistance, high Coulombic efficiency and good cycling/rate performance [26]. Therefore, constructing a suitable current collector is vitally important for high-performance LIBs, which, however, was ignored in previous studies at a large extend.

Conventional current collector for LIBs anodes was 2D planar Cu current collector which requires binder-containing slurry coating onto the surface. There are several existing problems. Noting that some anode materials undergo serious volume change upon cycling, the employment of planar Cu current collector may cause severe electrode pulverisation or falling off due to the confined contact area between planar current collector and active materials, which deteriorates battery performance. In addition, the introduction of non-conductive binders can increase the internal impedance of the battery, leading to large electrode polarization and decreased battery rate capability [27–30]. Exploiting 3D current collectors is an effective approach to deal with the above-mentioned problems. It has been demonstrated that 3D current collectors can enhance the electrochemical performance by min-

* Corresponding author.
*E-mail address:* liuwenbo_8338@163.com (W. Liu).

https://doi.org/10.1016/j.cclet.2024.109712
1001-8417/

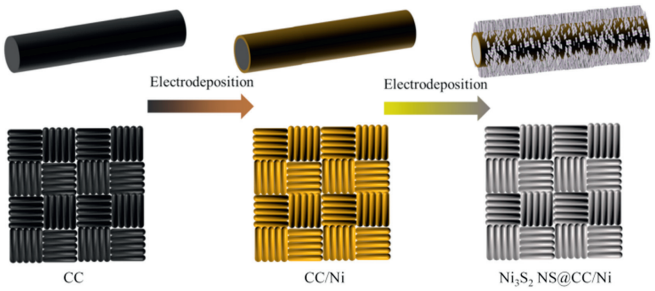


**Fig. 1.** Schematic design of synthesis procedure of the CC/Ni composite current collector and $Ni_3S_2$ NS@CC/Ni electrode.

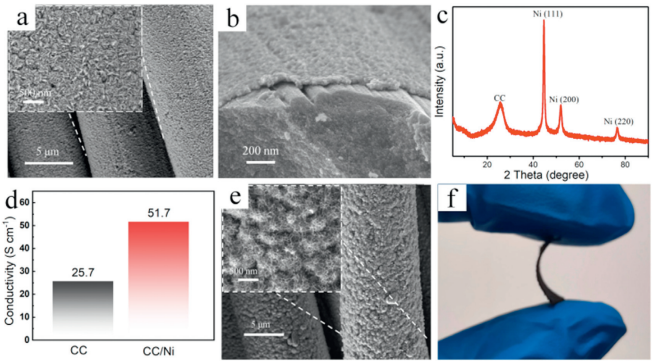


**Fig. 2.** (a) Top-view and (b) cross-section SEM images of CC/Ni composite current collector. (c) XRD pattern of CC/Ni composite current collector. (d) Comparison of electronic conductivity of CC and CC/Ni current collectors. (e) SEM image and high-resolution SEM image (insert) of $Ni_3S_2$ NS@CC/Ni electrode. (f) Photograph of the $Ni_3S_2$ NS@CC/Ni electrode illustrating the flexibility.

imizing the tortuosity of the ion/electron transport pathways to promote the ion/electron diffusion [31]. Besides, 3D current collectors with high surface area enable the active material layer of a thinner thickness under the same loading, which can relieve the mechanical crack caused by the huge volume expansion of the active materials upon battery operation [32]. The currently reported 3D current collectors mainly include metal and carbon materials [33,34]. Metal current collectors including Cu and Ni foams own exceptional electronic conductivity, yet feature relatively poor flexibility [35]. In addition, the stiff burrs derived from the thick metal collectors may pierce the separator and cause safety hazards [36]. 3D carbon current collectors feature good flexibility and mechanical strength, which are suitable for flexible energy storage devices [37]. However, the electronic conductivity was not as good as metal ones. Moreover, anodes using carbon current collectors with relatively smooth surface are still prone to terrible cycling stability due to the weak bonding between carbon current collector and active materials. Therefore, developing a highly conductive and stable flexible 3D current collector is significantly important and also very challenging.

According to the "skin effect", charges in the conductor are prone to concentrated on the surface [38]. Inspired by this, we developed a highly conductive and stable 3D flexible composite current collector simply by electrodepositing metallic Ni thin layer onto the carbon cloth (named as CC/Ni). Encouragingly, the tiny metallic Ni protrusions are homogeneously and densely distributed on the external CC substrate, which endows the 3D flexible CC/Ni composite current collector with exceptional electronic conductivity and mechanical stability. To verify its practical potential, as a proof-of-concept case, an array of $Ni_3S_2$ nanosheets was electrodeposited on CC/Ni (named as $Ni_3S_2$ NS@CC/Ni) testify the electrochemical performance. As expected, the prepared $Ni_3S_2$ NS@CC/Ni nanoporous anode delivers a high capacity of 2.31 mAh/cm$^2$ at 1 mA/cm$^2$ and 1.68 mAh/cm$^2$ at a high rate of 8 mA/cm$^2$.

Considering that charges in the conductor mainly distribute on the external surface, developing a current collector with highly conductive surface is vitally meaningful for high performance energy storage systems [38]. In this condition, the CC/Ni composite current collector was rationally designed and prepared through a facile electrodeposition method by directly depositing robust metallic Ni thin layer onto the carbon cloth, as the schematic illustration shown in Fig. 1. To demonstrate its real impact on the electrochemical performance, as a proof-of-concept case, $Ni_3S_2$ nanosheets were electrodeposited to the CC/Ni composite current collector to obtain $Ni_3S_2$ NS@CC/Ni nanoporous electrode for further measurements.

Fig. 2a shows the top-view scanning electron microscope (SEM) images of the CC/Ni composite current collector. Distinctly, the metallic Ni on the surface displays a dense and homogeneous protrusion morphology, which results from the inadequate growth of metallic Ni along the spiral dislocation. The cross-section SEM image of CC/Ni shown in Fig. 2b manifests that the thickness of metallic Ni layer is approximately 100 nm. More importantly, it can be discovered that the exposed Ni cross-section layer still in close contact with the carbon cloth even after cutting, proving the strong bonding force of metallic Ni layer with carbon substrate. Fig. 2c shows the XRD pattern of CC/Ni composite current collector. The three obvious diffraction peaks at $2\theta = 44.5°$, 51.8° and 76.3° correspond to the (220), (200) and (111) lattice planes of metallic Ni (PDF#04-8050), respectively [39]. In addition, a broad peak can be found at around 26°, which is related to the characteristic peak of carbon cloth component. The ingeniously designed rough metallic Ni surface on CC can not only enhance the electronic conductivity of the current collector, but also benefit to the further bonding with active materials. Fig. 2d compares the electronic conductivity of the CC and CC/Ni current collectors measured by digital four-probe meter. Excitingly, the CC/Ni composite current collector delivers significantly improved electronic conductivity of 51.7 S/cm compared to that of CC (25.7 S/cm). $Ni_3S_2$ nanosheets were then electrodeposited to the CC/Ni to obtain $Ni_3S_2$ NS@CC/Ni electrode. Fig. 2e shows the SEM image of the electrode. Obviously, the $Ni_3S_2$ active material shows 3D interconnected porous network with nanosheet structure evenly spread on the composite CC/Ni composite current collector, which is conductive to shorten the $Li^+$ transport distance, provide more active sites for $Li^+$ insertion, alleviate the volume expansion and improve the $Li^+$ diffusion kinetics. Additionally, the as-prepared $Ni_3S_2$ NS@CC/Ni electrode manifests exceptional flexibility, as the optical image illustrating the bending test shown in Fig. 2f.

The component and crystal structure of the $Ni_3S_2$ NS@CC/Ni electrode were further confirmed by transmission electron microscopy (TEM) technique. The TEM image shown in Fig. 3a manifests obvious contrast difference between light and dark. High-resolution TEM (HRTEM) image was provided to intensively identify the difference. As shown in Fig. 3b, the external lattice spacing of 0.237 and 0.281 nm can be assigned to the (003) and (110) crystal planes of $Ni_3S_2$, while the inner lattice spacing of 0.167 and 0.203 nm is related to the (200) and (111) crystal planes of metallic Ni [10]. Meanwhile, the lattice spacing of 0.335 nm corresponds to the (002) crystal plane of CC substrate. Fig. 3c shows the selected area electron diffraction (SAED) pattern of the $Ni_3S_2$ NS@CC/Ni electrode which shows obvious polycrystalline characteristic, corresponding well with the TEM result. Then, energy dispersive X-ray (EDX) energy spectra of TEM was performed to confirm the element distribution of Ni, S and C elements. As shown in Figs. 3d–g, Ni and S elements are homogeneously distributed, indicating the presence of $Ni_3S_2$. Besides, the content of Ni element

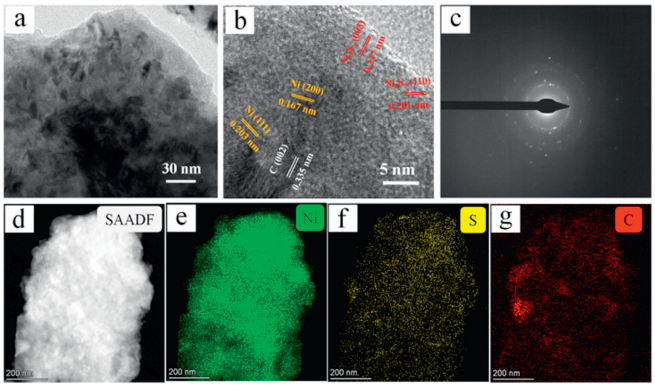


**Fig. 3.** (a) TEM image, (b) HRTEM image, and (c) SAED pattern of $Ni_3S_2$ NS@CC/Ni. (d–g) EDX elemental mapping images of the $Ni_3S_2$ NS@CC/Ni electrode.

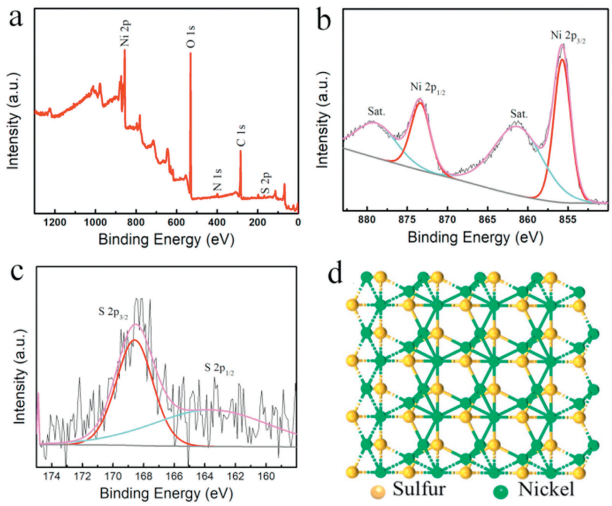


**Fig. 4.** (a) Survey XPS spectra, (b) Ni 2p high-resolution spectra, and (c) S 2p high-resolution XPS spectra of $Ni_3S_2$ NS@CC/Ni electrode. (d) Schematic of the crystal structure of $Ni_3S_2$.

was far more than S element, which maybe because of the presence of Ni layer on current collector. In addition, trace amounts of C element can also be detected which is associated with the CC current collector.

X-ray photoelectron spectroscopy (XPS) was employed to further analyze the elemental composition and valence distribution of the $Ni_3S_2$ NS@CC/Ni electrode. As displayed in Fig. 4a, S and Ni elements can be clearly detected in the survey XPS spectrum of the electrodes [33]. The high-resolution Ni 2p XPS spectrum in Fig. 4b can be divided into two peaks, where the spin-orbit splitting binding energies at 855.7 eV and 873.3 eV correspond to Ni $2p_{3/2}$ and Ni $2p_{1/2}$ characteristic peaks, respectively, while the peaks at 861.2 eV and 878.8 eV are related to the satellite peaks of Ni [12]. Two peaks at 163.3 eV and 168.6 eV are observed in the high-resolution S 2p XPS spectrum (Fig. 4c) which can be assigned to S $2p_{1/2}$ and S $2p_{3/2}$ peaks. In addition, it should be mentioned that $Ni_3S_2$ owns preferable electronic conductivity compared to other metal sulfide. This can be explained by the intrinsic crystal structure of $Ni_3S_2$ component. As shown in Fig. 4d, obviously, there is continuous Ni-Ni bonding networks throughout the structure, indicating the inherent metallic characteristic.

The binder-free $Ni_3S_2$ NS@CC/Ni electrodes were paired with metallic Li to evaluate their lithium storage performance. Fig. 5a shows the CV curve of $Ni_3S_2$ NS@CC/Ni electrode with a scan rate of 0.1 mV/s. During the first cathodic scan, peaks at 0.96 V and 0.82 V can be individually attributed to the formation of solid electrolyte interface (SEI) and initial embedding of $Li^+$ to form $Li_xNi_3S_2$ ($Ni_3S_2 + xLi^+ + xe^- \rightarrow Li_xNi_3S_2$) and metallic Ni ($Li_xNi_3S_2 + (4\text{-}x)Li^+ + (4\text{-}x)e^- \rightarrow 3Ni + 2Li_2S$). During the reverse anodic scan, the peaks observed at 1.01,1.39 and 2.00 V is attributed to the partial decomposition of SEI and multistep extraction of $Li^+$ ($3Ni + 2Li_2S \rightarrow Ni_3S_2 + 4Li^+ + 4e^-$), and the obvious peak at 0.2 V maybe relates to the CC [40,41]. It is worth noting that the subsequent discharge processes are somewhat different from the initial cycle due to the needless of SEI formation. Importantly, the CV curves for the second and third sweep cycles coincide well, indicating the highly reversible $Li^+$ insertion/extraction chemistry. The cycling performance of the electrode at 1 mA/cm$^2$ was shown in Fig. 5b. Excitingly, the binder-free $Ni_3S_2$ NS@CC/Ni electrode exhibits good cycling stability and high initial areal specific capacity (2.32 mAh/cm$^2$) due to the excellent structural stability and more exposed active sites. Even after 400 cycles, the electrode can still reach a reversible capacity of 1.63 mAh/cm$^2$ with a Coulombic efficiency of 99.5%. It should be noted that the capacity decay mainly occurs in the front 50 cycles, which may be ascribed to the partial flaking of $Ni_3S_2$ during the initial 50 cycles stemming from the high areal mass loading. The initial three charge-discharge curves of the electrode shown in Fig. S1 (Supporting information) are well overlapped, demonstrating the brilliant electrochemical stability. Fig. 5c compares the cycling performance of the prepared $Ni_3S_2$ NS@CC/Ni electrode with other reported $Ni_xS_y$-based anodes with different structure designs and current collectors [42–47]. Excitingly, the $Ni_3S_2$ NS@CC/Ni electrode exhibits the highest areal capacity compared to the other $Ni_xS_y$-based anodes (Table S1 in Supporting information). The rate capability of the $Ni_3S_2$ NS@CC/Ni electrode was shown in Fig. 5d. Comfortingly, the electrode achieves reversible capacities of 2.01, 1.85, 1.62 and 1.34 mAh/cm$^2$ at current densities of 1, 2, 4 and 8 mA/cm$^2$, respectively. More importantly, when the current density is back to 1 mA/cm$^2$, the reversible capacity returns to 1.90 mAh/cm$^2$. Note that the rate capability of the electrode stands out among the reported $Ni_xS_y$-based anodes with various structures and current collectors (Fig. S2 and Table S1 in Supporting information). The corresponding charge-discharge curves at various current densities were shown in Fig. 5e. It is obvious that the curve shape remains exactly the same even at a high current density of 8 mA/cm$^2$, indicating the fast reaction kinetics at high rates. The charge-discharge curves at different cycles shown in Fig. S3 (Supporting information) manifests almost coincide profile, demonstrating good cycling stability. Fig. S4 (Supporting information) displays the cycling performance of the $Ni_3S_2$ NS@CC/Ni electrode at a high rate of 4 mA/cm$^2$. The electrode still shows a high areal specific capacity of 1.31 mAh/cm$^2$ even after 500 cycles, achieving a capacity retention ratio of 76.6%.

Electrochemical impedance spectroscopy (EIS) was then employed to assess $Li^+$ and electron transfer kinetics of the electrodes. As shown in Fig. 5f, the $Ni_3S_2$ NS@CC/Ni electrode manifests a small charge transfer resistance ($R_{ct}$) of about 300 Ω before cycling, indicating a rapid ion transport. After cycling for 400 cycles, the Nyquist plot consists of two regions, where the first small semicircle in the high frequency range represents the resistance of SEI ($R_{SEI}$) and the second semicircle is the $R_{ct}$. Then, the values of $R_{SEI}$ and $R_{ct}$ are measured as 50 Ω and 200 Ω, respectively, manifesting improved $Li^+$ and electron transfer kinetics even after cycling due to the unique design of CC/Ni composite current collector. The post-mortem micro-structure of the $Ni_3S_2$ NS@CC/Ni electrode was shown in Fig. 5g and Fig. S5 (Supporting information) after 400 cycles. Gratifyingly, the $Ni_3S_2$ active material still maintains the original nanosheet structure without obvious shedding or fragmentation, convincingly indicating the excellent structural stability of the electrode enabled by the designed CC/Ni composite current collector. The practical feasibility was also demonstrated in $Ni_3S_2$ NS@CC/Ni||$LiFePO_4$ full cells. As shown in Fig. S6 (Supporting

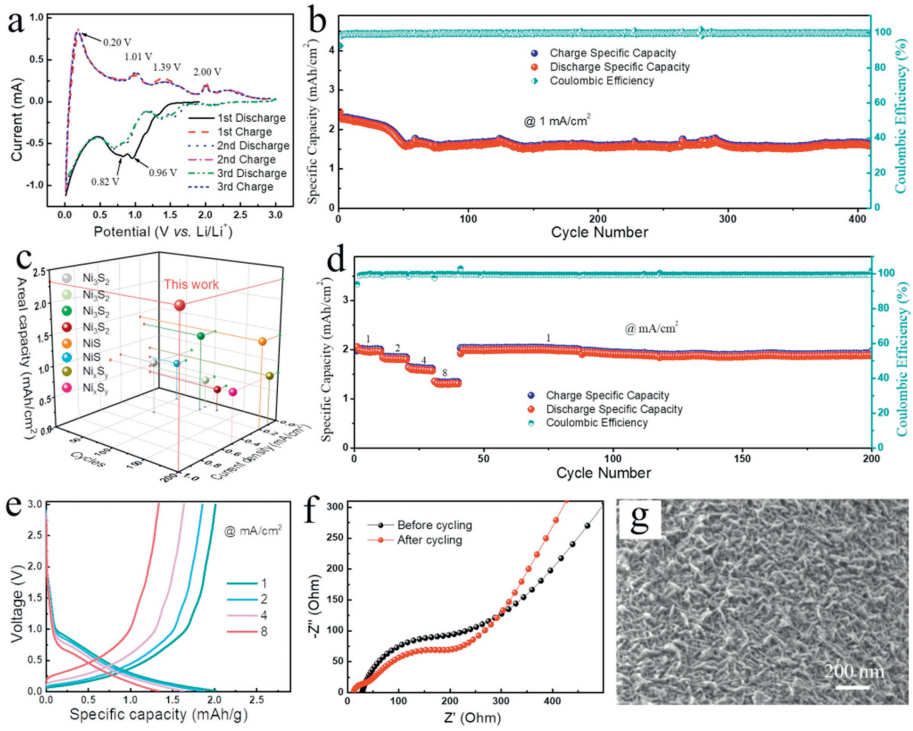


**Fig. 5.** (a) CV curves and (b) cycling performance of $Ni_3S_2$ NS@CC/Ni electrode. (c) Comparison of cycling performance of $Ni_3S_2$ NS@CC/Ni with other studies. (d) Rate performance, and (e) corresponding charge-discharge curves of $Ni_3S_2$ NS@CC/Ni electrodes. (f) Nyquist plots of the $Ni_3S_2$ NS@CC/Ni electrodes before and after cycling. (g) SEM image of $Ni_3S_2$ NS@CC/Ni electrode after cycling at 1 mA/cm$^2$.

information), the assembled full cell manifests stable cycling performance with a high specific capacity of 1.56 mAh/cm$^2$ after 80 cycles.

In summary, inspired by the "skin effect" in the conductor, a highly conductive and stable 3D flexible CC/Ni composite current collector was rationally designed and developed. Encouragingly, the tiny metallic Ni protrusions are homogeneously and densely distributed on the external CC substrate, which endows the 3D flexible CC/Ni composite current collector with exceptional electronic conductivity and mechanical stability. Moreover, the metallic Ni thin layer can strongly bond with the active components, ensuring the structural integrity of electrodes upon cycling. More importantly, the 3D network structure with large specific surface area provides abundant space to alleviate the volume expansion and more active sites for electrochemical reactions. As a result, the designed $Ni_3S_2$ NS@CC/Ni anode exhibits brilliant cycling (2.32 mAh/cm$^2$ at 1 mA/cm$^2$ and a high capacity retention of 69.4% after 400 cycles) and rate (1.68 mAh/cm$^2$ at 8 mA/cm$^2$) performance. This work offers a novel and universal approach to obtain highly conductive and stable 3D flexible electrodes towards high performance metal-ion batteries beyond LIBs.

## Declaration of competing interest

The authors declare that they have no known competing financial interests or personal relationships that could have appeared to influence the work reported in this paper.

## Acknowledgments

This work was financially supported by the National Natural Science Foundation of China (Nos. 52075351, 51604177), the National Key Research and Development Program of China (No. 2019YFA0705701), the National Funded Postdoctoral Researcher Program (No. GZC20231762), the Major S&T Infrastructure Construction Project of Sichuan Province (No. 2020-510000-73-01-441847), the International S&T Innovation Cooperation Program of Sichuan Province (No. 2020YFH0039), the Chengdu International S&T Cooperation Funded Project (Nos. 2020-GH02-00006-HZ, 2022-GH02-00027-HZ), the "1000 Talents Plan" of Sichuan Province, and the Talent Introduction Program of Sichuan University (No. YJ201410).

## Supplementary materials

Supplementary material associated with this article can be found, in the online version, at doi:10.1016/j.cclet.2024.109712.

## References

[1] T. Wang, J. Duan, B. Zhang, et al., Energy Environ. Sci. 15 (2022) 1325–1333.
[2] H. Liu, Q. Ye, D. Lei, et al., Energy Environ. Sci. 16 (2023) 1610–1619.
[3] H. Huang, L. Kong, W. Shuang, et al., Chin. Chem. Lett. 33 (2022) 1037–1041.
[4] W. Liu, P. Cheng, S. Zhang, et al., Metall. Mater. Trans. A 51 (2020) 2536–2548.
[5] X. Yan, H. Kang, P. Cheng, et al., EcoMat 4 (2022) e12208.
[6] J. Gao, X. Wang, Y. Huang, et al., J. Alloys Compd. 853 (2021) 157354.
[7] Y. Zhou, Y. Zhu, B. Xu, et al., Nano-Micro Lett. 11 (2019) 1–9.
[8] J. Li, J. Cao, X. Li, et al., Electrochim. Acta 332 (2020) 135446.
[9] Y. Gao, W. Zhou, W. Li, et al., J. Alloys Compd. 845 (2020) 155590.
[10] J. Li, J. Li, Z. Ding, et al., Chem. Eng. J. 378 (2019) 122108.
[11] J.L. Xu, L. Liu, Y.H. Sun, et al., J. Alloys Compd. 835 (2020) 155418.
[12] D. Zhu, S. Li, J. Huang, et al., J. Alloys Compd. 859 (2021) 158246.
[13] J. Lee, C. Choi, H. Lee, et al., Adv. Energy Mater. 12 (2022) 2103138.
[14] H. Liu, J. Wang, W. Hua, et al., Energy Environ. Sci. 15 (2022) 1872–1881.
[15] H. Liu, J.G. Wang, W. Hua, et al., Adv. Sci. 8 (2021) 2102612.
[16] X. Huo, L. Xu, K. Xie, et al., Adv. Energy Mater. 13 (2023) 2203066.
[17] Y. Fang, D. Luan, Y. Chen, et al., Angew. Chem. Int. Ed. 59 (2020) 2644–2648.
[18] Z. Li, M. He, B. Bo, et al., Energy Environ. Mater. 4 (2021) 577–585.
[19] H. Yoon, D. Park, H.J. Song, et al., ACS Sustain. Chen. Eng. 9 (2021) 8487–8496.
[20] J. Li, Z. Ding, J. Li, et al., Chem. Eng. J. 407 (2021) 127199.
[21] H.S. Mohamed, C.F. Li, L. Wu, et al., Chem. Eng. J. 407 (2021) 126941.
[22] Y. Yang, J. Xia, X. Guan, et al., Small 18 (2022) 2204970.
[23] Y. Gao, F. Qiao, J. You, et al., Nat. Commun. 13 (2022) 5.
[24] S. Chen, R. Tao, J. Tu, et al., Adv. Funct. Mater. 31 (2021) 2101199.
[25] J.B. Goodenough, Y. Kim, Chem. Mater. 22 (2010) 587–603.

[26] P. Zhu, D. Gastol, J. Marshall, et al., J. Power Sources 485 (2021) 229321.
[27] X. Kang, G. Fu, X. Wang, et al., Chin. Chem. Lett. 32 (2021) 938–942.
[28] Z. Zhang, Y. Hou, S. Zhang, et al., Chin. Chem. Lett. 29 (2018) 1656–1660.
[29] M.H. Nazir, A. Rahil, E. Partenie, et al., Battery Energy 1 (2022) 20220022.
[30] T. Xu, D. Wang, Z. Li, et al., Nano-Micro Lett. 14 (2022) 126.
[31] Y. Yu, L. Gu, X. Lang, et al., Adv. Mater. 23 (2011) 2443–2447.
[32] Q. Yun, Y.B. He, W. Lv, et al., Adv. Mater. 28 (2016) 6932–6939.
[33] S. Fu, X. Yang, P. Zhao, et al., ACS Appl. Energy Mater. 5 (2022) 5159–5169.
[34] Z. Zhang, P. Zhu, C. Li, et al., Chin. Chem. Lett. 32 (2021) 154–157.
[35] S. Jin, Y. Jiang, H. Ji, et al., Adv. Mater. 30 (2018) 1802014.
[36] S. Zhang, Y. Xing, T. Jiang, et al., J. Power Sources 196 (2011) 6915–6919.
[37] S. Li, H. Xiao, J. Zhou, et al., Nanoscale Adv. 14 (2022) 16560–16571.
[38] Y. Wang, G. Zhang, R. Qiu, et al., IEEE Trans. Transp. Electr. 7 (2021) 883–891.
[39] J. Xu, Y. Sun, M. Lu, et al., Sci. China Mater. 62 (2019) 699–710.
[40] M.J. Choi, J.H. Baek, J.Y. Kim, et al., Battery Energy 2 (2023) 20230010.
[41] Y. Li, L. Zhang, H.Y. Yen, et al., Nano-Micro Lett. 15 (2023) 63.
[42] W. Duan, W. Yan, X. Yan, et al., J. Power Sources 293 (2015) 706–711.
[43] C. Wang, Q. Han, R. Xie, et al., Electrochim. Acta 331 (2020) 135383.
[44] X. Dong, Z.P. Deng, L.H. Huo, et al., J. Alloys Compd. 788 (2019) 984–992.
[45] M. Vadivazhagan, S. NK, K.J.E. Nallathamby, et al., Energy Fuels 35 (2021) 8991–9000.
[46] M. Guan, Z. Li, J. Ouyang, et al., Mater. Today Commun. 31 (2022) 103652.
[47] S. Jiang, M. Mao, M. Pang, et al., Appl. Surf. Sci. 635 (2023) 157697.